

A reanalysis of radioisotope measurements of the ${}^9\text{Be}(\gamma, n){}^8\text{Be}$ cross-section

Alan E. Robinson

Fermi National Accelerator Laboratory, Batavia, Illinois, USA^{*}

(Dated: May 10, 2022)

The ${}^9\text{Be}(\gamma, n){}^8\text{Be}$ reaction is enhanced by a near threshold $1/2^+$ state. Contradictions between existing measurements of this reaction cross-section affect calculations of astrophysical r-process yields, dark matter detector calibrations, and the theory of the nuclear structure of ${}^9\text{Be}$. Select well-documented radioisotope ${}^9\text{Be}(\gamma, n)$ source yield measurements have been reanalyzed, providing a set of high-accuracy independently measured cross sections. A Breit-Wigner fit of these corrected measurements yields $E_R = 1738.8^{+5.0}_{-4.2}$ keV, $\Gamma_\gamma = 0.771^{+0.055}_{-0.044}$ eV, and $\Gamma_n = 268^{+40}_{-33}$ keV for the $1/2^+$ state. The fit favors a resonant $1/2^+$ state, but a virtual state is not excluded.

The contribution of the near threshold $1/2^+$ state to the ${}^9\text{Be}(\gamma, n){}^8\text{Be}$ reaction is important for several problems in nuclear and astrophysics. This cross-section is used to calculate the formation rate of ${}^9\text{Be}$ via the ${}^4\text{He}(an, \gamma){}^9\text{Be}$ reaction, one of the most important light-element reactions for r-process nucleosynthesis [1]. Neutrons from ${}^{88}\text{Y}/\text{Be}$ and other radioisotope sources using the ${}^9\text{Be}(\gamma, n){}^8\text{Be}$ reaction near threshold are being used widely for dark matter detector energy scale and yield calibrations [2, 3], as these low energy neutrons closely mimic dark matter recoils in detectors [4]. Recent studies of the nuclear structure of ${}^9\text{Be}$ suggest that three-cluster dynamics are important and that astrophysical ${}^9\text{Be}$ production may proceed via a single step, with a much larger production rate at low energies than that calculated by the two-step process via ${}^8\text{Be}$ [5, 6]. The predictions of three-cluster models depends on whether the state is virtual or a resonance [7].

There is little agreement between many measurements of the ${}^9\text{Be}(\gamma, n){}^8\text{Be}$ reaction, especially near the $1/2^+$ state. The yields of radioisotope photoneutron sources provide the simplest method to measure the cross-section [8–15]. Other measurements using bremsstrahlung photon beams [16, 17], and more recently using inverse Compton photon beams [18, 19], such as the High-Intensity γ Source (HI γ S), provide cross sections over a range of energies while sacrificing energy resolution and simplicity in experimental design. These techniques compare the absolute incoming photon and outgoing neutron fluxes. Accurate cross-section measurements require knowledge of the absolute photon source strengths, the neutron detection efficiencies, and the photon energy spectra. These three quantities are more easily measured with radioisotope sources.

The cross-section can also be found using the inelastic scattering of charged particles [20–26]. These measurements require significant background subtraction and extrapolation to low momentum transfer to recover a cross-section. A selection of measured cross sections and their 50% level disagreements are shown in Figure 1.

Despite the simplicity of radioisotope measurements

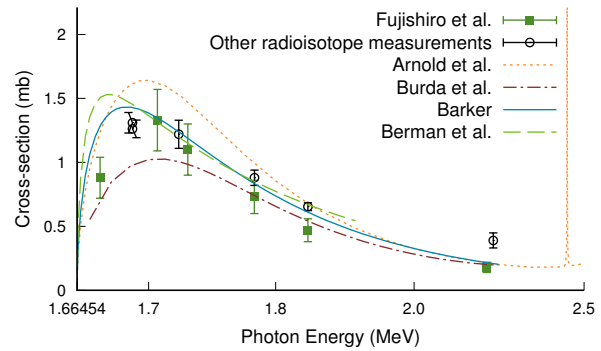


Figure 1. A selection of existing near-threshold cross section measurements of the ${}^9\text{Be}(\gamma, n){}^8\text{Be}$ reaction [11–15, 17, 19, 26]. Lines show the cross-section from fitted Breit-Wigner parameters. The parameters from Barker [27] were a fit to data from [24].

of the ${}^9\text{Be}(\gamma, n){}^8\text{Be}$ cross-section, discrepancies among these are as severe as those from more complicated experiments at accelerator facilities. Most of the radioisotope measurements were performed in the 1940s, 50s, and 60s, before high precision neutron standards, cross sections, and simulation programs were available. Fortunately, several of these experiments have been well documented with results that are traceable to modern calibrations. This paper will apply corrections to these originally measured cross-section values to construct a trusted set of high-accuracy measured cross sections near the ${}^9\text{Be}(\gamma, n)$ threshold.

I. RADIOISOTOPE MEASUREMENTS

A. John and Prosser

John and Prosser [14] used the MnSO_4 bath technique [28] to measure the yield of a ${}^{124}\text{Sb}$ source and traced their measured neutron yield to NBS-1, the world's most precisely calibrated neutron standard. The strength of their ${}^{124}\text{Sb}$ source was measured using a NaI crystal.

A list of corrections to the measurement was provided in John and Prosser [14, Table I], and is reproduced with

* fbfree@fnal.gov

Item	from John and Prosser		Recalculated	
	Correction (%)	Uncertainty (%)	Correction (%)	Uncertainty (%)
1. Gamma-ray source strength				
(a) peak-to-total ratio	—	5.0	+3.88	3.5
(b) subtraction of other γ -ray lines	—	2.0	+0.42	2.0
(c) half-life of ^{124}Sb	—	0.8	-0.8	0.1
2. Neutron source strength				
(a) absolute strength of NBS source	—	3.0	+0.4	0.85
(b) neutron escape from MnSO_4 bath	-0.9	0.3	-0.84	0.05
(c) capture of fast neutrons in bath	-2.8	0.5	-2.34	0.12
(d) neutron counting statistics	—	0.8	—	0.8
3. Finite source size	-0.6	< 0.1	—	—
4. Attenuation of gamma rays in Be shell	+2.5	< 0.1	—	—
5. Neutrons produced by other γ -ray lines	-4.4	1.0	-2.04	—
6. Source geometry effects			+2.65	2.0
Total Correction	-6.2%		1.012	
Overall uncertainty (square root of sum of squares)		6.4%		4.7%

Table I. Corrections to the neutron yield of an $^{124}\text{Sb}/\text{Be}$ source, reproduced from Table I in John and Prosser [14] and extended with recalculated corrections. The finite source size (3) and gamma attenuation (4) effects are combined and reported with other source geometry effects (6) in an MCNPX-Polimi simulation in the reevaluation. See text for descriptions of other recalculated corrections.

corrections in Table I. The largest correction and uncertainty is to the peak to total ratio in the 2" thick 1.75" diameter NaI crystal. An MCNP simulation of the detector with a 1.41 MeV threshold gives a ratio of 0.2244 versus the originally used ratio of 0.216. A 3.5% uncertainty ($5\%/\sqrt{2}$) in the photon source strength is retained to account for uncertainties subdominant to those specified in the paper.

In 1962, only the 1.69 MeV and the 2.09 MeV lines were well established in the high energy ^{124}Sb photon spectrum [29]. John and Prosser subtracted from the measured photon yield the contribution from the Compton tail from the 2.09-MeV line. Several percent and sub-percent intensity sub-threshold photon lines have been found since 1962 that lie within the NaI detector resolution of the 1.69-MeV peak [30]. Assuming a NaI(Tl) detector with 5.4% energy resolution at the peak, an additional 0.42% background subtraction is applied. The ^{124}Sb half-life has been revised to 60.20 ± 0.03 days from 60.4 ± 0.2 days. As the neutron counting significantly preceded the photon counting, the decay correction was increased.

To calibrate the neutron yield against NBS-1, an intermediate $^{226}\text{Ra}/\text{Be}$ (α, n) source was used. Correction factors for this comparison were recalculated using MCNPX-Polimi simulations, replacing the original analytic corrections made by John and Prosser. Photoneutrons were generated in the simulation by generating photons and simulating the $^9\text{Be}(\gamma, n)^8\text{Be}$ reaction. An MCNP library [31] based on the cross section measured by Arnold *et al.* [19] was used. The $^{226}\text{Ra}/\text{Be}$ neu-

tron spectrum used to generate source particles in the simulation was calculated using the JENDL-AN/05 evaluated $^9\text{Be}(\alpha, n)$ cross section [32] and a modified version of the SOURCES-4C program [33, 34]. Neutron propagation was modelled using the ENDF/B-VII.1 cross section libraries [35]. The ratio of the number of neutrons captured on manganese and the number of neutrons produced was calculated from these simulations and used to compare the $^{226}\text{Ra}/\text{Be}$ and $^{124}\text{Sb}/\text{Be}$ neutron yield measurements. The largest difference in yield is due to the increased probability of neutron capture on sulfur and oxygen for high energy neutrons from the $^{226}\text{Ra}/\text{Be}$ source.

The absolute neutron yield of the NBS-1 neutron source has been revised slightly upward and the yield uncertainty reduced since its 1955 calibration [28, 36].

Radioisotope source yields, the number of neutrons produced per decay, may be expressed as the sum of the photon branching ratios α_i and cross sections σ_i . For John and Prosser's $^{124}\text{Sb}/\text{Be}$ measurement, a yield of $\sum_i \alpha_i \sigma_i = 0.678 \pm 0.032$ is found. This expression ignores the contribution of bremsstrahlung photons from high energy β decays. The bremsstrahlung contribution was calculated and found to be negligible for ^{124}Sb and other isotopes considered here.

John and Prosser compared their $^{124}\text{Sb}/\text{Be}$ source to $^{28}\text{Al}/\text{Be}$ and $^{206}\text{Bi}/\text{Be}$ sources. As their neutron emission rate was too weak to measure using the MnSO_4 bath method, a 'Long Counter' was used for the comparison. MCNPX-Polimi simulations of the Harwell IV Long Counter [37] found that the counter had equal sen-

sitivity (within 1%) to neutrons from each of the three sources. John and Prosser's 3% correction to the sensitivity of neutrons from $^{28}\text{Al}/\text{Be}$ was reduced to 0.7%. No other corrections to the cross section beyond those in the original paper were added. The reported cross sections were converted into the following neutron yield ratios.

$$\frac{\sigma(1779 \text{ keV})}{\sum_i \alpha_i \sigma_i(^{124}\text{Sb})} = 1.311 \pm 0.043$$

$$\frac{\sum_i \alpha_i \sigma_i(^{206}\text{Bi})}{\sum_i \alpha_i \sigma_i(^{124}\text{Sb})} = 0.620 \pm 0.030$$

B. Gibbons *et al.*

Gibbons *et al.* [13] measured both $^{124}\text{Sb}/\text{Be}$ and $^{88}\text{Y}/\text{Be}$ neutron sources to high precision using different techniques from those of John and Prosser. The decay rate of their sources were determined using a 4π ionization counter. Their neutron source strengths were measured using a 5-foot diameter graphite moderating sphere and BF_3 thermal neutron detectors. The neutron count rate was calibrated against a source traceable to NBS-1.

Gibbons *et al.* [13, Table I] had calculated several corrections to the their source yield. These corrections were recalculated, with only the source strength of the NBS neutron source requiring an update, increasing the yield by 0.4% and reducing its uncertainty to 0.85%. With this update, their yield was $\sum_i \alpha_i \sigma_i(^{124}\text{Sb}) = 0.669 \pm 0.029$ and $\sum_i \alpha_i \sigma_i(^{88}\text{Y}) = 0.660 \pm 0.029$.

C. Snell *et al.*

Snell *et al.* [11] measured the neutron yields from beryllium and deuterium targets using ^{72}Ga and ^{24}Na radioisotopes. Both isotopes produce photons above the 2.2 MeV deuterium dissociation threshold. The absolute neutron yield and the ratio of beryllium to deuterium neutron yields was measured for each radioisotope. The measured ratio can be compared to the well known modern cross section for the photodissociation of deuterium [35].

Their neutrons were measured by sampling epithermal neutrons in large volume of paraffin moderator using indium foil sandwiched between two cadmium foils. The activated indium was counted using a thin-walled Geiger counter. The neutron energy dependence of the neutron yield measurements of Snell *et al.* has been validated using MCNPX-Polimi [38]. One additional correction, for the thermalization of neutrons reentering the deuterium or beryllium from the surrounding moderator, leads to an small additional loss of efficiency. The ratio of the detection efficiency for each source was recalculated. The original uncertainty in the relative source activity is retained, and it dominates the total uncertainty of 3%. For $^{24}\text{Na}/\text{Be}$ $\sum_i \alpha_i \sigma_i = 0.620$ mb while for $^{72}\text{Ga}/\text{Be}$ $\sum_i \alpha_i \sigma_i = 0.171$ mb.

Isotope	E_γ (keV)	Intensity (%)	Ref.
^{58}Co	1674.7	0.53	[15]
	1674.725(7)	0.517(10)	[39]
^{105}Ru	1705.2	0.113	[15]
	1698.1(2)	0.076(14)	[40]
	1721.36(15)	0.033(9)	
	others > 1664 keV	0.0017(12)	
^{65}Ni	1724.9	0.39	[15]
	1724.92(6)	0.399(12)	[41]
^{28}Al	1778.9	100	[15]
	1778.987(15)	100	[42]
	1836.0	99.34	[15]
^{88}Y	1836.063(12)	99.2(3)	[43]
	2734.0(5)	0.71(7)	
	3219.7(20)	0.0070(20)	
	2167.6	42.4	[15]
^{38}Cl	2167.54(7)	44.4	[44]
	others > 1664 keV	0.041(32)	

Table II. Radioisotope sources of > 1.67 MeV photons used in Fujishiro *et al.* [15]. The given updated values of the photon branching ratios were used in this reevaluation.

D. Fujishiro *et al.*

The measurements of Fujishiro *et al.* [15] are the most recent radioisotope measurements of the $^9\text{Be}(\gamma, n)^8\text{Be}$ and have heavily influenced modern evaluations of the cross section [26, 45, 46]. Fujishiro *et al.* selected a large variety of short-lived radioisotopes that produce photons with energies near the $1/2^+$ state, shown in Table II. Paraffin embedded BF_3 detectors were used to measure the neutron flux.

The neutron energy dependence of this detector was originally calculated using a one-dimensional Monte Carlo code and normalized to the flux of a $^{24}\text{Na}-\text{D}_2\text{O}$ neutron source. The relative neutron energy dependence was verified using three-dimensional MCNPX-Polimi simulations and found to generally match the shape of the function reported by Fujishiro *et al.*. Only for 8 keV neutrons from ^{58}Co was a different efficiency found; an relative efficiency 5% lower than that of Fujishiro *et al.* will be used.

The expected absolute sensitivity of the neutron detector used by Fujishiro *et al.* could not be verified using simulations given limited information about either the gas density of their BF_3 detectors or the details of their detector calibration. Only the ratios of their measured cross sections will be used.

Fujishiro *et al.* did not consider the uncertainty in the photon branching ratios of each isotope when reporting the $^9\text{Be}(\gamma, n)$ cross section. Table II shows the high energy branching ratios they used, and the most recent evaluated branching ratio for each isotope. The updated branching ratios differ by up to 13% from those originally used. A $\pm 21\%$ uncertainty in the high energy photon branching ratio has been found to dominate all other uncertainties for the neutron yield of ^{105}Ru .

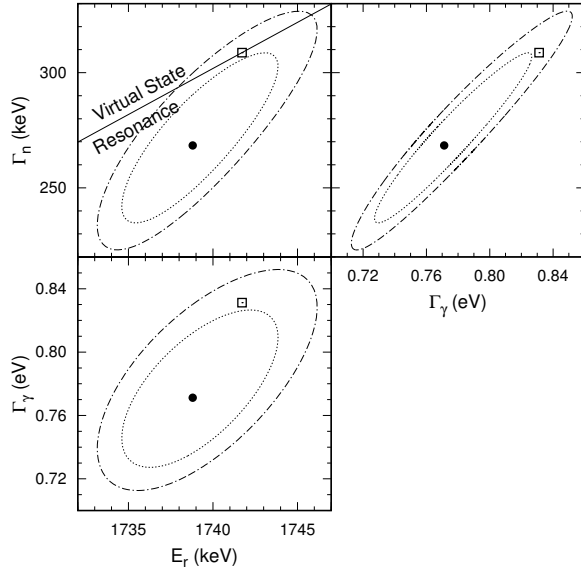


Figure 2. Fit Breit-Wigner parameters to the $1/2^+$ state. Best fit parameters (solid circles) are $E_R = 1738.8_{-4.2}^{+5.0}$ keV, $\Gamma_\gamma = 0.771_{-0.044}^{+0.055}$ eV, and $\Gamma_n = 268_{-33}^{+40}$ keV. 68% and 95% confidence regions are shown. A virtual state would exist if $\Gamma \approx \Gamma_n > E_R - S_n$ [5]. The best fit virtual state solution is shown (open squares).

II. FIT

The ${}^9\text{Be}(\gamma, n){}^8\text{Be}$ cross section was fit using least squares to a sum of isolated Breit-Wigner states. The $1/2^+$ state was fit to the form

$$\sigma_{1/2^+} = \frac{\pi(\hbar c)^2}{4E_\gamma^2} \frac{\Gamma_n \sqrt{\frac{E_\gamma - S_n}{E_R - S_n}} \Gamma_\gamma \left(\frac{E_\gamma}{E_R}\right)^3}{(E_\gamma - E_R)^2 + \frac{E_\gamma - S_n}{E_R - S_n} (\Gamma_n/2)^2} \quad (1)$$

where the neutron separation energy $S_n = 1664.54$ keV. The contribution from other resonances was fixed to that measured by Arnold *et al.* [19]. It is assumed there is negligible contribution from the $\alpha + \alpha + n$ continuum or nonresonant processes. The photon energies, branching ratios, and measured neutron yield for each radioisotope measurement was input to the fit. The yields measured by Fujishiro *et al.* were allowed to float freely. The χ^2 contribution of the ${}^{206}\text{Bi}/\text{Be}$ and ${}^{28}\text{Al}/\text{Be}$ yield measurements of John and Prosser [14] were calculated using their ratio to the ${}^{124}\text{Sb}/\text{Be}$ source yield. The absolute source yields were used for all other measurements. The ${}^{24}\text{Na}/\text{Be}$ source yield from Snell *et al.* [11] was excluded as it is well above the $1/2^+$ state, although its agreement with Arnold *et al.* validates the use of their cross sections for the higher energy resonances. Regardless, the fit to the $1/2^+$ state is stable to 10% scale variations in the cross section contribution from higher energy resonances. Results from the fit are shown in Figures 2 and 3.

As shown in Figure 2, a virtual state is disfavored at an 80% confidence level, but not excluded by the radioiso-

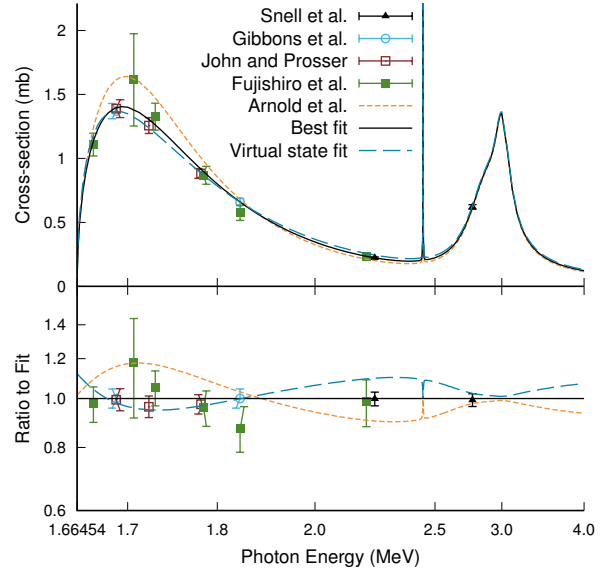


Figure 3. Reanalyzed cross sections from radioisotope measurements of the ${}^9\text{Be}(\gamma, n){}^8\text{Be}$ cross section. Only the cross sections for the highest intensity photon energy of each radioisotope are shown, assuming that ratio to the cross sections at other photon energies equal the best fit ratios. The absolute yield of the measurements by Fujishiro *et al.* [15] are floated. The highest energy measurement by Snell *et al.* [11] of the ${}^{24}\text{Na}/\text{Be}$ source yield was not included in the fit. It is used to validate the contribution of higher energy resonances as measured by Arnold *et al.* [19].

Isotope	$t_{1/2}$	$E_\gamma (\alpha_i)$ (keV)	$E_n^{\text{c.m.}}$ (keV)	Yield ($\sum_i \alpha_i \sigma_i$) (mb)
${}^{58}\text{Co}$	70.86 d	1674.73 (0.517%)	9.05	$5.9 \pm 0.5 \times 10^{-3}$
${}^{88}\text{Y}$	106.63 d	1836.06 (99.2%)	171.52	0.654 ± 0.024
		2734.0 (0.71%)	1069.46	$4.0 \pm 0.4 \times 10^{-3}$
		3219.7 (0.0070%)	1555.16	$3.0 \pm 0.9 \times 10^{-5}$
		Total		0.658 ± 0.024
${}^{124}\text{Sb}$	60.20 d	1690.97 (47.57%)	26.43	$0.664 \pm 0.$
		2090.93 (5.49%)	426.39	$0.0150 \pm 0.$
		others (0.52%)		0.00255
		Total		0.682 ± 0.020
${}^{207}\text{Bi}$	31.55 y	1770.23 (6.87%)	105.69	0.0657 ± 0.0027
${}^{226}\text{Ra}$	1600 y	1729.60 (2.878%)	57.78	0.0354 ± 0.0022
		1764.49 (15.30%)	99.95	0.152 ± 0.006
		1847.43 (2.025%)	162.42	0.01262 ± 0.00028
		2204.06 (4.924%)	539.52	0.0110 ± 0.0010
		others (9.69%)		0.0176
		Total		0.228 ± 0.008

Table III. Neutron centre-of-mass energies ($E_n^{\text{c.m.}}$) and yields for commercially available isotopes used in near threshold photoneutron sources. The neutron yield is the product of the ${}^9\text{Be}(\gamma, n)$ cross section σ_i and the photon branching fraction α_i for each photon energy E_γ . Photon yields energies and half-lives, including those of decay chain daughter isotopes, are from [30, 39, 43, 47–49].

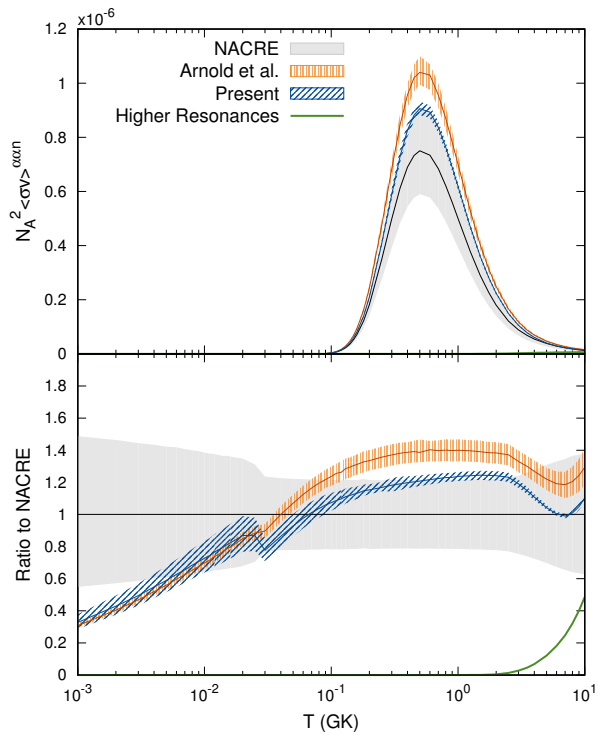


Figure 4. Calculated rate from the two step ${}^4\text{He}(\alpha n, \gamma){}^9\text{Be}$ fusion reaction compared to previous evaluations [19, 46]. Bands show $\pm 1\sigma$ uncertainties.

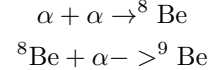
tope data. The precise measurements of the ${}^{124}\text{Sb}/\text{Be}$ and ${}^{72}\text{Ga}/\text{Be}$ source yields provide a strong constraint on the ratio of the cross section in the $1/2^+$ resonance peak and tail respectively.

For use in dark matter detector calibrations, the yields and uncertainties of individual commercially available photoneutron sources are given in Table III.

III. ASTROPHYSICAL PRODUCTION

The ${}^9\text{Be}(\gamma, n){}^8\text{Be}$ cross section may be used to calculate the dominant two step contribution to the astrophysical production rate of the $\alpha(\alpha n, \gamma){}^9\text{Be}$ reaction. The

reaction proceeds via,



with both ${}^8\text{Be}$ and ${}^9\text{Be}$ in their ground state. A direct three-body reaction is possible and may dominate the reaction rate at low temperatures [6], but high-sensitivity searches for this process have not demonstrated its existence [50]. The thermal production rate by the two-step process in a double integral over the energy of two Maxwell-Boltzmann distributed collision velocities, the cross sections for the two subprocesses, and the mean lifetime of the ${}^8\text{Be}$ nucleus, where the ${}^8\text{Be}$ nucleus may be produced off-shell [46].

The ${}^8\text{Be}(\alpha, \gamma){}^9\text{Be}$ reaction is related by the reciprocity theorem to the ${}^9\text{Be}(\gamma, \alpha){}^8\text{Be}$ cross section, as described by Arnold *et al.* [19]. The cross section for elastic $\alpha + \alpha$ scattering via the ${}^8\text{Be}$ compound state is taken from [51], with resonance width $\Gamma_{\alpha\alpha} = 0.557 \pm 0.025$ and resonant energy $E_r = 92.03$ keV.

Table IV shows the adopted ${}^9\text{Be}$ astrophysical production rate while Figure 4 shows this rate in comparison with the calculations of NACRE [46] and Arnold *et al.* [19]. At low and high temperatures, the rate follows that of Arnold *et al.*, while at the astrophysically relevant temperatures of 1 GK to 5 GK, the new rate is nearly the average of those from NACRE and Arnold *et al.*.

IV. SUMMARY

Radioisotope source yield measurements of the near threshold $1/2^+$ state of the ${}^9\text{Be}(\gamma, n){}^8\text{Be}$ reaction cross section have been reanalyzed. After reanalysis, these measurements are self-consistent and provide the most precise experimental bounds of the Breit-Wigner parameters, with absolute cross section uncertainties near 3%. The best fit to the cross section indicates that the $1/2^+$ state is a resonance, although a virtual state interpretation is only weakly disfavored.

ACKNOWLEDGMENTS

This work was derived from my thesis under the guidance of Juan Collar at the University of Chicago, and completed with the support of the Fermi Research Alliance, LLC under Contract No. DeAC0207CH11359 with the United States Department of Energy.

[1] T. Sasaqui, T. Kajino, G. J. Mathews, K. Otsuki, and T. Nakamura, *Astrophys. J.* **634**, 1173 (2005).
[2] L. Hsu, At Calibration of Low Energy Particle Detectors Workshop, Chicago, 2015 (unpublished).
[3] C. Amole *et al.* (PICO Collaboration), ArXiv e-prints (2015), arXiv:1510.07754.
[4] J. I. Collar, *Phys. Rev. Lett.* **110**, 211101 (2013).

T (GK)	$N_A^2 \langle \sigma v \rangle^{\alpha\alpha n}$						T (GK)	$N_A^2 \langle \sigma v \rangle^{\alpha\alpha n}$					
	-2σ	-1σ	Adopted	$+1\sigma$	$+2\sigma$	Exp		-2σ	-1σ	Adopted	$+1\sigma$	$+2\sigma$	Exp
0.001	1.060	1.118	1.280	1.475	1.562	-59	0.14	3.788	3.849	3.991	4.162	4.237	-8
0.002	0.890	0.938	1.074	1.237	1.309	-47	0.15	5.608	5.691	5.887	6.125	6.229	-8
0.003	5.539	5.840	6.679	7.687	8.138	-42	0.16	7.842	7.952	8.207	8.519	8.657	-8
0.004	2.539	2.677	3.060	3.520	3.725	-38	0.18	1.345	1.361	1.399	1.447	1.468	-7
0.005	1.033	1.089	1.244	1.430	1.513	-35	0.2	2.025	2.048	2.098	2.163	2.192	-7
0.006	1.020	1.075	1.228	1.410	1.492	-33	0.25	3.940	3.980	4.066	4.182	4.234	-7
0.007	4.029	4.245	4.845	5.563	5.884	-32	0.3	5.625	5.705	5.897	6.126	6.223	-7
0.008	0.842	0.887	1.012	1.162	1.228	-30	0.35	6.974	7.074	7.312	7.584	7.697	-7
0.009	1.108	1.166	1.330	1.525	1.612	-29	0.4	7.921	8.025	8.266	8.542	8.656	-7
0.01	1.025	1.079	1.230	1.409	1.489	-28	0.45	8.483	8.586	8.819	9.087	9.196	-7
0.011	0.721	0.759	0.864	0.990	1.046	-27	0.5	8.716	8.824	9.061	9.326	9.432	-7
0.012	4.074	4.288	4.880	5.587	5.901	-27	0.6	8.609	8.713	8.933	9.171	9.264	-7
0.013	1.926	2.027	2.306	2.638	2.786	-26	0.7	8.073	8.170	8.370	8.581	8.660	-7
0.014	0.786	0.827	0.940	1.074	1.134	-25	0.8	7.393	7.478	7.646	7.822	7.888	-7
0.015	2.831	2.978	3.384	3.866	4.080	-25	0.9	6.665	6.743	6.896	7.052	7.109	-7
0.016	0.918	0.966	1.096	1.252	1.321	-24	1	5.973	6.045	6.184	6.323	6.372	-7
0.018	0.745	0.783	0.888	1.013	1.068	-23	1.25	4.527	4.582	4.690	4.794	4.830	-7
0.02	4.595	4.829	5.468	6.225	6.561	-23	1.5	3.469	3.512	3.597	3.677	3.704	-7
0.025	2.204	2.310	2.595	2.929	3.078	-21	1.75	2.706	2.740	2.808	2.873	2.895	-7
0.03	3.435	3.584	3.924	4.312	4.494	-19	2	2.154	2.180	2.234	2.286	2.304	-7
0.04	1.461	1.516	1.642	1.785	1.851	-15	2.5	1.438	1.455	1.490	1.525	1.537	-7
0.05	2.155	2.226	2.395	2.587	2.673	-13	3	1.022	1.034	1.056	1.078	1.087	-7
0.06	5.700	5.870	6.279	6.744	6.951	-12	3.5	7.627	7.704	7.848	8.000	8.053	-8
0.07	5.686	5.841	6.214	6.639	6.827	-11	4	5.918	5.976	6.074	6.179	6.216	-8
0.08	3.097	3.174	3.361	3.575	3.669	-10	5	3.904	3.945	3.990	4.050	4.072	-8
0.09	1.130	1.156	1.219	1.291	1.323	-9	6	2.821	2.856	2.890	2.925	2.945	-8
0.1	3.121	3.188	3.348	3.534	3.615	-9	7	2.174	2.206	2.239	2.271	2.294	-8
0.11	7.054	7.193	7.528	7.919	8.090	-9	8	1.764	1.795	1.827	1.859	1.884	-8
0.12	1.373	1.398	1.459	1.530	1.561	-8	9	1.489	1.520	1.552	1.584	1.610	-8
0.13	2.384	2.425	2.522	2.637	2.688	-8	10	1.293	1.323	1.355	1.387	1.413	-8

Table IV. Calculated rate from the two step ${}^4\text{He}(\alpha n, \gamma){}^9\text{Be}$ fusion reaction versus temperature including 68% and 95% confidence intervals.

- [5] V. D. Efros, P. v. Neumann-Cosel, and A. Richter, Phys. Rev. C **89**, 027301 (2014).
- [6] J. Casal, M. Rodríguez-Gallardo, J. M. Arias, and I. J. Thompson, Phys. Rev. C **90**, 044304 (2014).
- [7] M. Odsuren, Y. Kikuchi, T. Myo, M. Aikawa, and K. Katō, Phys. Rev. C **92**, 014322 (2015).
- [8] J. Chadwick and M. Goldhaber, Proc. R. Soc. A **151**, 479 (1935).
- [9] H. von Halban, C. R. Acad. Sci. **1938/01**, 1170 (1938).
- [10] B. Russell, D. Sachs, A. Wattenberg, and R. Fields, Phys. Rev. **73**, 545 (1948).
- [11] A. H. Snell, E. C. Barker, and R. L. Sternberg, Phys. Rev. **80**, 637 (1950).
- [12] B. Hamermesh and C. Kimball, Phys. Rev. **90**, 1063 (1953).
- [13] J. H. Gibbons, R. L. Macklin, J. B. Marion, and H. W. Schmitt, Phys. Rev. **114**, 1319 (1959).
- [14] W. John and J. M. Prosser, Phys. Rev. **127**, 231 (1962).
- [15] M. Fujishiro, T. Tabata, K. Okamoto, and T. Tsujimoto, Can. J. Phys. **60**, 1672 (1982).
- [16] M. J. Jakobson, Phys. Rev. **123**, 229 (1961).
- [17] B. L. Berman, R. L. V. Hemert, and C. D. Bowman, Phys. Rev. **163**, 958 (1967).
- [18] H. Utsunomiya, Y. Yonezawa, H. Akimune, T. Yamagata, M. Ohta, M. Fujishiro, H. Toyokawa, and H. Ohgaki, Phys. Rev. C **63**, 018801 (2000).
- [19] C. W. Arnold, T. B. Clegg, C. Iliadis, H. J. Karwowski, G. C. Rich, J. R. Tompkins, and C. R. Howell, Phys. Rev. C **85**, 044605 (2012).
- [20] K. V. Tucker SN, Treacy PB, Aust. J. Phys. **23**, 651 (1970).
- [21] R. R. Spencer, G. C. Phillips, and T. E. Young, Nucl. Phys. **21**, 310 (1960).
- [22] H. N. Ngoc, M. Hors, and J. P. Y. Jorba, Nucl. Phys. **42**, 62 (1963).

- [23] H.-G. Clerc, K. J. Wetzel, and E. Spamer, Nucl. Phys. **A120**, 441 (1968).
- [24] G. Kuechler, A. Richter, and W. von Witsch, Z. Phys. A **326**, 447 (1987).
- [25] S. Dixit *et al.*, Phys. Rev. C **43**, 1758 (1991).
- [26] O. Burda, P. von Neumann-Cosel, A. Richter, C. Forssén, and B. A. Brown, Phys. Rev. C **82**, 015808 (2010).
- [27] F. C. Barker, Aust. J. Phys. **53**, 247 (2000).
- [28] E. D. McGarry and E. W. Boswell, National Bureau of Standards Special Publication No. 250-18, 1988.
- [29] R. Girgis and R. V. Leshout, Physica **25**, 133 (1959).
- [30] J. Katakura and Z. D. Wu, Nuclear Data Sheets **109**, 1655 (2008).
- [31] A. E. Robinson, Phys. Rev. C **89**, 032801 (2014).
- [32] T. Murata, H. Matsunobu, and K. Shibata, JAEA-Research Report No. 2006-052, 2006.
- [33] W. B. Wilson *et al.*, Los Alamos National Laboratory Report No. LA-UR-02-1839, 2002 (unpublished).
- [34] A. E. Robinson, Ph.D. thesis, University of Chicago (2015).
- [35] M. B. Chadwick, M. Herman, P. Obložinský, M. E. Dunn, Y. Danon, A. C. Kahler, D. L. Smith, *et al.*, Nuclear Data Sheets **112**, 2887 (2011).
- [36] J. W. De Juren and J. Chin, J. Res. Nat. Bur. Stand. **55**, 311 (1955).
- [37] W. D. Allen, Atomic Energy Research Establishment Report No. NP/R 1667, 1955.
- [38] E. Padovani, S. A. Pozzi, S. D. Clarke, and E. C. Miller, Documentation for Radiation Safety Informational Computer Center code package CCC-791, 2012 (unpublished).
- [39] C. D. Nesaraja, S. D. Geraedts, and B. Singh, Nuclear Data Sheets **111**, 897 (2010).
- [40] D. D. Frenne and E. Jacobs, Nuclear Data Sheets **105**, 775 (2005).
- [41] E. Browne and J. K. Tuli, Nuclear Data Sheets **111**, 2425 (2010).
- [42] M. S. Basunia, Nuclear Data Sheets **114**, 1189 (2013).
- [43] E. A. McCutchan and A. A. Sonzogni, Nuclear Data Sheets **115**, 135 (2014).
- [44] J. A. Cameron and B. Singh, Nuclear Data Sheets **109**, 1 (2008).
- [45] F. C. Barker, Can. J. Phys. **61**, 1371 (1983).
- [46] C. Angulo *et al.*, Nucl. Phys. A **656**, 3 (1999).
- [47] F. G. Kondev and S. Lalkovski, Nuclear Data Sheets **112**, 707 (2011).
- [48] S. Singh, A. K. Jain, and J. K. Tuli, Nuclear Data Sheets **112**, 2851 (2011).
- [49] S.-C. Wu, Nuclear Data Sheets **110**, 681 (2009).
- [50] D. E. Alburger, R. E. Chrien, R. J. Sutter, and J. F. Wishart, Phys. Rev. C **70**, 064611 (2004).
- [51] S. Wüstenbecker, H. Becker, H. Ebbing, W. Schulte, M. Berheide, M. Buschmann, C. Rolfs, G. Mitchell, and J. Schweitzer, Z. Phys. A **344**, 205 (1992).